Chemical Science

ROYAL SOCIETY OF CHEMISTRY

EDGE ARTICLE

View Article Online
View Journal | View Issue

Cite this: *Chem. Sci.*, 2025, **16**, 21991

All publication charges for this article have been paid for by the Royal Society of Chemistry

Received 13th August 2025
Accepted 3rd October 2025

DOI: 10.1039/d5sc06168g

rsc.li/chemical-science

Installation of cationic phosphorus on dimethyldihydropyrene photoswitches: expanding the atomic repertoire towards far-red photoswitching in water

Manik Lal Maity,[a] Sayan Chandra,[a] Samyadeb Mahato[ab] and Subhajit Bandyopadhyay *[a]

We have synthesized for the first time a small library of negative photochromic dimethyldihydropyrene phosphonium salts (**DHPPs**) that can be activated by red and far-red (up to 740 nm) photons in a quantitative manner in the so-called "biological window". The intriguing feature of this particular class is their remarkably fast response in fully aqueous media with an improved ring-opening quantum yield. Additionally, the reversal can be activated upon visible (blue) light irradiation and also under thermal conditions in a quantitative manner, achieving efficient bidirectional visible light-mediated switching rendering this particular class of photoswitches even more attractive towards their potential application in biological premises. Additionally, all-photonic orthogonal photoswitching of a mixture of conventional unsubstituted **DHP** and one of our modified **DHPP** derivatives provides a demonstration of multifunctional molecular logic operations.

Introduction

Molecular photoswitches have recently emerged as versatile tools for diverse biological applications, including regulation of ion channels,[1–3] modulating protein activity,[4–6] controlling cellular signaling,[7–9] photo-regulated bio-mimetic catalysis[10–13] and in photopharmacology.[14–16] Employing light as an external bio-orthogonal stimulus provides unparalleled precision in three-dimensional space and time for modulating biological processes. In this context, red and near-infrared (NIR) light, particularly, is advantageous due to its benign nature and superior tissue penetration depth compared to ultraviolet (UV) irradiation. In addition, the deployment of photoswitches in biological systems also requires their efficient performance in a fully aqueous environment with robust switching. However, widely used photoswitches such as azobenzenes,[17,18] spiropyrans,[19–21] and diarylethenes[22,23] often use UV light in one of the reversible steps in the photoswitching process. Frequently, many of these systems suffer from poor aqueous solubility, thus exhibiting suboptimal switching and degradation in water. While progress has been made either in enhancing water solubility[24–32] or in developing visible and near-IR-responsive photoswitches,[33,34] there remains a strong demand for designing systems that not only exhibit red and far-red light activation but also demonstrate efficient reversible switching in a fully aqueous environment.

Background

Negative (inverse) T-type photochromic systems[35] can be promising candidates for potential biomedical applications due to their unique photophysical properties. Negative photochromic systems can be activated by visible light, which is less damaging than the high-energy UV light often required by positive-photochromic systems. When exposed to visible light, these systems show almost complete decoloration of their thermodynamically stable, colored form. This leads to increased optical transparency and improved light penetration in the forward step with the progress of the switching. T-type photoswitching allows the system to thermally revert to its original state under physiological conditions, eliminating the need for extra light input. This offers a further advantage. Thus, for a negative T-type photochromic system, the thermodynamically stable isomer absorbs light selectively at longer wavelengths, enabling deeper tissue penetration and more precise photo-regulation in biological environments.[36] Beyond biomedical applications, depending upon the rate of the thermal relaxation, T-type photochromic systems play a vital role in developing photochromic lenses,[37] fluorescence switches,[38,39] and real-time holographic materials.[40,41]

In light of these considerations, we direct our attention to a dimethyldihydropyrene–cyclophanediene (**DHP–CPD**) system

[a]*Department of Chemical Sciences, Indian Institute of Science Education and Research Kolkata, Mohanpur, 741246, India. E-mail: sb1@iiserkol.ac.in*

[b]*Department of Chemistry, Simon Fraser University, Burnaby, British Columbia V5A 1S6, Canada*

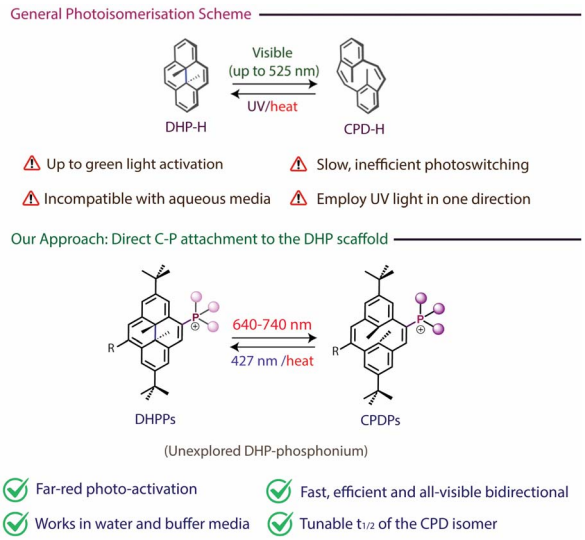

Fig. 1 General photoisomerization scheme of the DHP-switch and its limitations; our approach to addressing the problems.

(Fig. 1) that exhibits negative photochromism.[42] The green-"closed" *trans*-10*b*,10*c*-dimethyl-10*b*,10*c*-dihydropyrene (**DHP**) comprises a rigid, extended 14π-electron framework, with two methyl groups positioned axially opposite to one another on either side of the aromatic plane. Upon exposure to visible light, it undergoes 6π-electrocyclic conrotatory ring-opening to generate a colorless, stepped-like "open" cyclophanediene (**CPD**) isomer through the opening of a central carbon–carbon bond. The reverse reaction can be triggered either thermally or photo-chemically through UV (254 nm) irradiation (Fig. 1).[42] Despite its intriguing properties, this particular class of photochromic systems has attracted relatively limited attention, likely owing to the synthetic complexity, moderate efficiency of the ring-opening process, and poor compatibility with aqueous environments. However, efforts have been made towards the functionalization of the **DHP** scaffold.[43–47] The photophysical properties were improved as a result of these structural modifications, as reflected in their increased photoisomerization efficiency,[48–50] tunable absorption profiles,[36,51] and enhanced thermal stability of the metastable isomer.[44,45]

Strategy

Despite a handful of the aforementioned advancements of the photophysical properties of the **DHP** systems, efforts towards the attachment of heteroatoms directly to the **DHP** scaffold remains significantly underexplored, despite their promising potential to finely tune the electronic properties, enhance water solubility, and shift switching wavelengths beyond what traditional carbon-linked analogs can offer. In this context, the direct attachment of a phosphorus heteroatom to the **DHP** scaffold represents an unexplored avenue for functional diversification. In addition to that, recognizing the widespread utility of the tetraarylphosphonium moiety across diverse fields,[52–56] we synthesized and studied the photophysical properties of the previously unexplored **DHP**-based phosphonium salts, wherein the electron-deficient cationic phosphorus is directly attached to the **DHP** scaffold (Fig. 1). We envisioned that this strategic modification could address four key challenges associated with the **DHP** system for prospective biological applications: (1) the cationic phosphonium salt acting as a hydrophilic moiety could render the otherwise hydrophobic **DHP** scaffold water-soluble. (2) The electron-deficient phosphonium [Hammett parameters (σ_p): $PMe_3^+ \rightarrow 0.73$, $PPh_2Me^+ \rightarrow 1.18$][57] could favor charge transfer in the excited states from the electron-rich **DHP** motif, likely shifting the wavelength of the absorbance and enabling photoisomerization with low-energy photons. (3) The ring-opening quantum yield of the **DHP**-phosphonium systems could be significantly enhanced compared to that of the parent **DHP**, owing to the presence of a directly attached electron-deficient phosphonium scaffold.[47] (4) The inclusion of an aryl phosphonium group could impart a strong emissive nature as observed in other aryl phosphonium compounds.[58]

In this study, we wish to report for the first time the synthesis and improved photo-physical properties of a series of cationic dimethyldihydropyrene phosphonium salts (**DHPPs**), demonstrating highly efficient ring-opening/closing photoisomerization reactions that can be exclusively controlled bidirectionally with visible light: 640–740 nm for ring-opening, and 427 nm for ring-closing (and also thermally) in an efficient manner in fully aqueous media. Additionally, in-depth theoretical calculations were employed to rationalize the experimental findings. We have also synthesized the neutral **DHP**-phosphine oxide and observed a noticeable improvement of the activation energy and the thermal half-life of the metastable isomer compared to the cationic derivatives.

Results and discussion

In order to explore the structure–property relationship, we first aimed to synthesize cationic **DHP**-triphenylphosphonium salt **DHPP-1**. The synthesis was accomplished in three successive steps from the precursor 2,7-di-*t*-butyl-*trans*-10*b*,10*c*-dihydropyrene (**DHP**). The parent **DHP** was synthesized following the reported synthetic protocol.[44] The **DHP** was then brominated (**6**) in a quantitative manner using 1 equiv. of NBS.[59] The desired compound **DHPP-1** was then obtained by the classical Pd-catalyzed cross-coupling reaction developed by Charette and Marcoux between the aryl bromide and triphenylphosphine in dry toluene (Scheme 1).[60] Column chromatography with 1% MeOH in CH_2Cl_2 provided compound **DHPP-1** as a brown solid in 61% yield (detailed synthetic procedures are available in the SI, Page S4). The cationic **DHPP-1** was then explored as a negative photoswitch to operate in the fully aqueous media. The characteristic UV-vis absorption spectrum of compound **DHPP-1** in water displayed four major electronic transitions located at 360 nm ($\varepsilon = 46\,500\ M^{-1}\ cm^{-1}$), 401 nm ($\varepsilon = 42\,000\ M^{-1}\ cm^{-1}$), 504 nm ($\varepsilon = 7800\ M^{-1}\ cm^{-1}$), and 651 nm ($\varepsilon = 4500\ M^{-1}\ cm^{-1}$). All the absorption bands of **DHPP-1** are significantly red-shifted compared to those of the parent unsubstituted **DHP**, and the molar extinction coefficient for the lowest energy band is more pronounced than that of the parent **DHP** (Fig. S36 and S37). Interestingly, upon irradiation of **DHPP-1** (35 μM in water) with

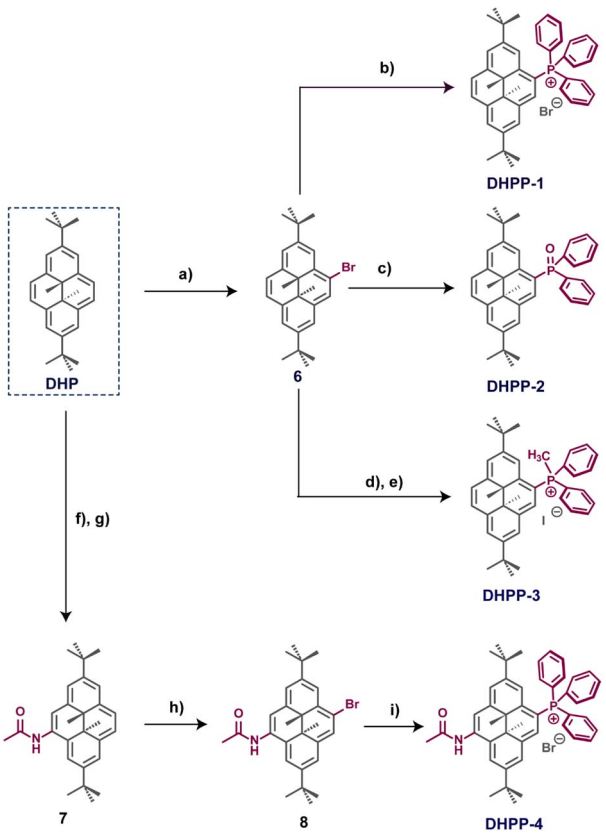

Scheme 1 Synthesis of **DHPPs**. Reaction conditions: (a) NBS (1 equiv.), DMF/CH_2Cl_2, −50 °C; (b) PPh_3, $Pd_2(dba)_3$, dry toluene, 130 °C; (c) PPh_2HO (1 equiv.), $Pd(OAc)_2$, dppf, Cs_2CO_3, dry DMF; (d) *n*-BuLi, TMEDA, −50 °C, dry Et_2O, PPh_2Cl; (e) MeI, dry CH_2Cl_2; (f) Ac_2O, $Cu(NO_3)_2$, 0 °C; (g) Zn dust, NaOAc; (h) NBS (1 equiv.), DMF/CH_2Cl_2, −50 °C; (i) PPh_3, $Pd_2(dba)_3$, dry toluene, 130 °C.

640 nm (red) light (0.6 W cm^{-2}), the color of the solution changed rapidly from brownish green to pale yellow with a gradual decrease of the characteristic absorption bands in the visible region corresponding to the closed isomer (Fig. 2a and b) along with a simultaneous enhancement of the band at 268 nm, characteristics of the colorless open **CPDP-1** isomer with a clean isosbestic point at 306 nm. The photoswitching performance of **DHPP-1** was then determined by measuring the PSS distribution and the ring-opening quantum yield.[32,61] To our delight, we observed almost quantitative conversion of the closed isomer to the corresponding open isomer (upon 640 nm light irradiation) with an estimated quantum yield of ∼3.3% (in water), which is 5.5-fold higher compared to that of the parent **DHP** (0.6% in cyclohexane).[62] However, the superiority of this new system lies in the use of water as the solvent and biocompatible 640 nm red-light as the switching wavelength (Fig. S54 and Table S1). The appearance of the open cyclophanediene **CPDP-1** was monitored by the growth of a band in the UV region, along with a residual absorption at 402 nm, which tails out up to 456 nm. Therefore, we wondered if the **CPDP-1** → **DHPP-1** reversal could be achieved by blue light. Indeed, the irradiation of the open isomer with 427 nm blue LED light (0.6 W cm^{-2}) within seconds reverted back to ∼54% of the closed isomer (Fig. S33) in the photostationary state (PSS). Also, upon exposure to 254 nm light, a better photoreversal (∼77% closed isomer) was achieved. However, the extent of reversal can be significantly improved upon thermal activation, and ∼85% of the closed isomer was recovered (Fig. 2c). This scenario was not observed for the normal unsubstituted **DHP**, which doesn't undergo ring-opening upon exposure to 640 nm light. This strategic modification led to its all-visible light-induced reversible switching. Unlike the conventional unsubstituted **DHP**, it can undergo ring-opening with up to 640 nm light in a fast and efficient way, and reversal can be accomplished with 427 nm visible (blue) light. The PSS distribution for the forward and reverse isomerization with the **DHPP-1** at various wavelengths of light was monitored and tabulated in Table 1. The photoisomerization event was also monitored by ^1H and ^{31}P NMR spectroscopy (Fig. 2d). Upon exposure to 640 nm red light for 15 min, the peaks in ^1H NMR at δ −3.93 ppm and −3.97 ppm, attributed to the internal methyl protons, were found to be diminished completely with the evolution of two new peaks at δ 1.47 ppm and 1.29 ppm, respectively, corresponding to the same set of protons, confirming the cleavage of the central C–C bond (Fig. 2d). The signature peaks for the *t*-butyl groups of **DHPP-1** that appeared at δ 1.65 ppm and 1.18 ppm diminished completely upon isomerization, and appeared at δ 1.26 ppm and 0.94 ppm, respectively, indicating the generation of the **CPDP-1** isomer (Fig. 2d). The quaternary phosphorus atom also exhibited a significant shift upon photoisomerization. In ^{31}P NMR, the peak at δ 22.37 ppm was found to have completely vanished upon 640 nm light irradiation and appeared at δ 24.32 ppm, characteristic of the **CPDP-1** isomer (Fig. 2e). In order to estimate the thermal stability of the open isomer, variable temperature kinetic experiments were performed. The activation energy for the open **CPDP-1** was estimated to be 18.9 ± 0.9 kcal mol^{-1}, and the thermal half-life was determined to be ∼27 h at 298 K (Table 1). Notably, the UV-vis absorption spectra of **DHPP-1** remained similar in the organic solvents and water.

Role of the cationic phosphonium unit

The serendipitous red-light activation of the phosphonium-attached **DHPP-1** can be explained by considering the electron-withdrawing effect of the cationic triphenylphosphonium moiety and thus promoting the photoisomerization of **DHPP-1** with low-energy light in a fast manner, directly from the lowest excited singlet state (*vide infra*). Thus, in order to have a better understanding of the role of the cationic phosphonium in the photochemical performance of the **DHP** scaffold, it was essential to synthesize a structurally similar uncharged analog of **DHPP-1**. Therefore, the uncharged air-stable phosphine oxide **DHPP-2** was synthesized. The uncharged derivative **DHPP-2** can be obtained from monobromo **DHP** (**6**) by the Pd-catalyzed cross-coupling reaction between aryl bromide and diphenylphosphine oxide in 71% yield (Scheme 1, also see the SI for the detailed procedure). The green crystals of **DHPP-2** (CCDC: 2444320) can be obtained by the slow evaporation of a saturated solution of **DHPP-2** in acetonitrile. In comparison to the cationic species **DHPP-1**, all

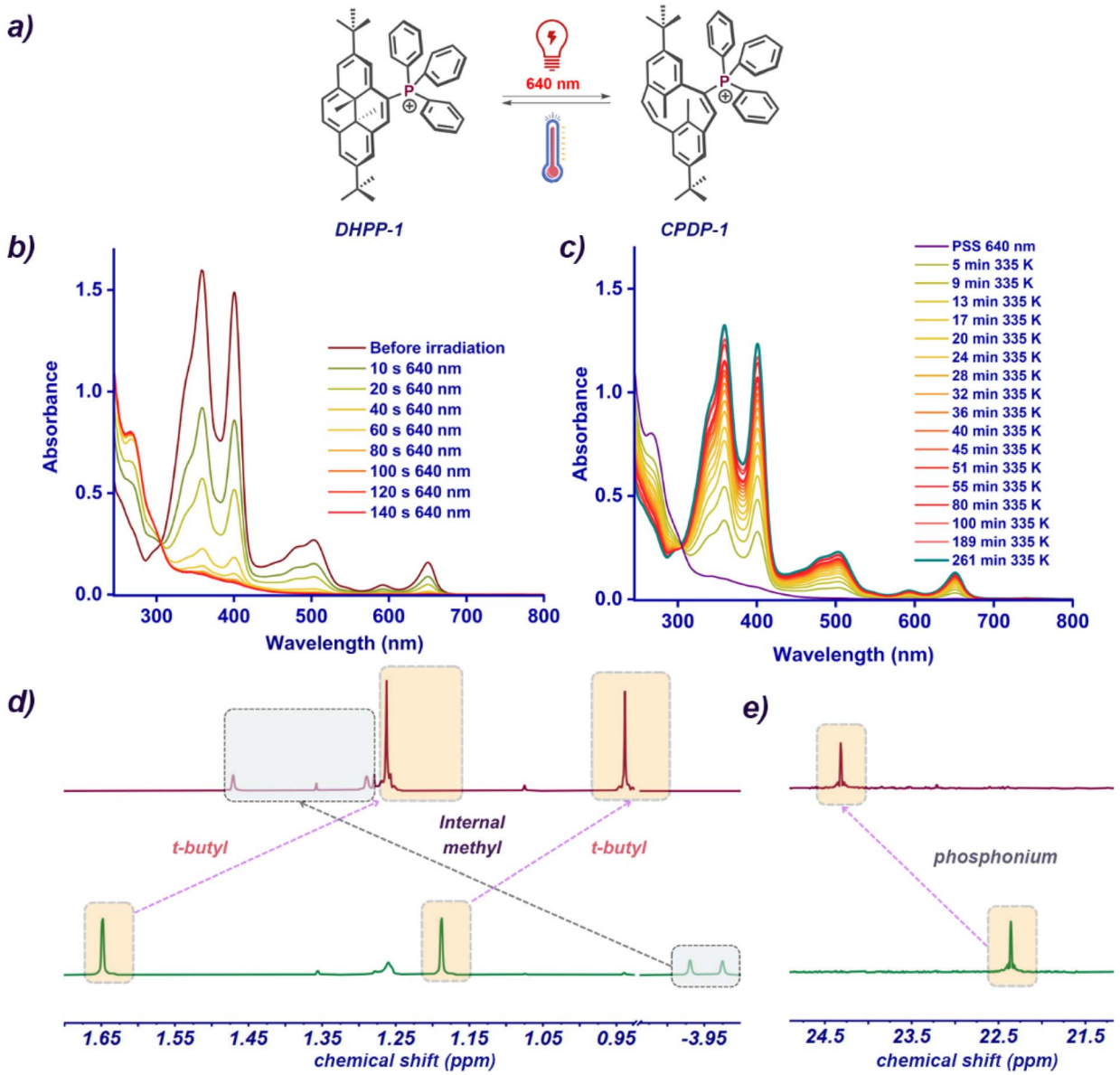

Fig. 2 (a) Photoisomerization and thermal reversal isomerization scheme of **DHPP-1** (Br^- as the counteranion). (b) Forward photoisomerization of **DHPP-1** (35 μM in water) upon 640 nm red light irradiation. (c) Thermal reverse isomerization for the formation of the **DHPP-1** isomer at 335 K in water. (d) Partial ^{1}H-NMR spectra of **DHPP-1** in CD_3CN depicting photoisomerization, (e) ^{31}P-NMR spectra of **DHPP-1** in CD_3CN depicting photoisomerization.

the electronic transitions of neutral **DHPP-2** [350 nm (ε = 32 600 M^{-1} cm^{-1}), 390 nm (ε = 22 800 M^{-1} cm^{-1}), 492 nm (ε = 4500 M^{-1} cm^{-1}), and 648 nm (ε = 1300 M^{-1} cm^{-1})] were blue-shifted (Fig. 3a and b). Interestingly, neutral **DHPP-2** can also be quantitatively photoisomerized to the colorless **CPDP-2** isomer even with 640 nm red light. However, the ring-opening of neutral **DHPP-2** was substantially slower than that of the cationic phosphonium salt **DHPP-1**, with an estimated ring-opening quantum yield of ~0.95% (Fig. S55 and Table S2) upon 640 nm irradiation, indicating the pivotal role of the directly attached cationic moiety in the faster ring-opening of the **DHP** scaffold. However, unlike compound **CPDP-1**, the reversal of **CPDP-2** was not activated by 427 nm visible (blue) light, which was obvious from the absence of any absorption band in the visible region of **CPDP-2** in the UV-vis absorption spectra (Fig. 3b). The reversal of the open cyclophanediene **CPDP-2** was initiated either by 254 nm light irradiation or thermally. The energy barrier of activation for the open **CPDP-2** → **DHPP-2** conversion was estimated to be 24.7 ± 1.1 kcal mol^{-1}, and the thermal half-life of the **CPDP-2** was observed to be ~66 h at 298 K (Table 1), reasonably higher than that of cationic **CPDP-1**.

Replacing the phenyl with a methyl group

Ensuring the positive charge on the phosphorus atom has a direct influence on the switching speed and the all-visible

Table 1 Photophysical properties of the synthesized derivatives (in water), PSS composition for the forward (ring-opening) and reverse (ring-closing) photoisomerization steps, percentage of thermal reversal (ring-closing) from isomerization kinetics data, half-lives of the metastable isomers and ring-opening quantum yield of **DHPPs**

Compounds	Absorption maxima (ε [10^4 M^{-1} cm^{-1}]) (nm) $S_0 \rightarrow S_1$ (ε_1), $S_0 \rightarrow S_2$ (ε_2), $S_0 \rightarrow S_3$ (ε_3), $S_0 \rightarrow S_4$ (ε_4)	PSS distribution (% of open isomer)				% of thermal reversal	Activation energy (E_a) for thermal reversal (kcal mol^{-1})	Half-life ($t_{1/2}$) at 298 K by extrapolation (h)	Ring-opening quantum yield (%)
		740[c] nm	640[c] nm	427[d] nm	254[d] nm				
DHPP-1[b]	651 (0.45), 504 (0.78), 401 (4.2), 360 (4.65)	N/A	Quant.	54	77	85	18.91 ± 0.97	27	3.3
DHPP-2[a]	648 (0.13), 492 (0.45), 390 (2.28), 350 (3.26)	N/A	Quant.	N/A	81	Quant.	24.70 ± 1.11	66	0.95
DHPP-3[b]	650 (0.23), 502 (0.41), 398 (2.6), 357 (3.1)	N/A	Quant.	70	80	Quant.	21.86 ± 0.48	17	8.5
DHPP-4[b]	659 (0.46), 506 (0.74), 404 (4.5), 364 (3.8)	Quant.	Quant.	45	88	Quant.	21.27 ± 0.57	11	5.7

[a] For solubility reasons, photoswitching of **DHPP-2** was performed in acetonitrile. [b] Performed in 100% HPLC water. [c] PSS determined from NMR spectroscopy. [d] PSS determined from UV-vis spectroscopy at a wavelength where the absorbance of one isomer is negligible.

bidirectionality of the **DHP** scaffold. So, we explored the effect of the alkyl group on the cationic phosphorus by replacing one of the phenyl groups with a methyl substituent to synthesize methyl di-phenyl phosphonium **DHPP-3**. The desired compound **DHPP-3** can be obtained in a two-step reaction from **6** (Scheme 1) with an overall yield of 52% (detailed synthetic procedures are available in the SI, Scheme S1). Suitable crystals (CCDC: 2442745) were obtained upon anion exchange with PF_6^-, confirming the attachment of the cationic phosphorus to the **DHP** scaffold. The UV-vis absorption spectrum of the cationic species **DHPP-3** in water displays four major transitions located at 357 nm (ε = 31 000 M^{-1} cm^{-1}), 398 nm (ε = 26 000 M^{-1} cm^{-1}), 502 nm (ε = 4100 M^{-1} cm^{-1}), and 650 nm (ε = 2300 M^{-1} cm^{-1}), quite similar to that of the analogous **DHPP-1**. Similarly, cationic **DHPP-3** can be photoisomerized with 640 nm red light in water in a quantitative manner (Fig. S21 and S22). Surprisingly, it was observed that ring-opening of **DHPP-3** was even faster than that of compound **DHPP-1**, with an estimated quantum yield of ~8.5% (Fig. S56 and Table S3). Also, the calculated ring-opening quantum yield of **DHPP-3** in water was significantly higher than that of uncharged **DHPP-2**, again demonstrating the faster ring-opening of the **DHP** scaffold upon incorporation of the cationic moiety. The photo-generated **CPDP-3** isomer has a residual absorption in the visible region located at 400 nm, which extends up to 460 nm. Thus, upon irradiation of the open **CPDP-3** isomer with 427 nm blue light almost instantly reverts back to ~70% of the closed isomer (Fig. S34, 4b and Table 1). The reversal of the open **CPDP-3** could also be performed by 254 nm light irradiation or even thermally. Indeed, the extent of thermal reversal of **CPDP-3** was also quantitative (Table 1). The activation energy for the open **CPDP-3** was estimated to be 22 ± 0.5 kcal mol^{-1}, and the thermal half-life of the **CPDP-3** was calculated to be ~17 h at 298 K (Table 1).

Role of counter-anions

In order to explore the role of the counter-anions in the photoswitching performance of the synthesized **DHPPs**, crystalline **DHPP-3** having PF_6^- as the other counter-anion was also synthesized and its photoswitching performance in water was investigated. Notably, the absorption profile along with the photoswitching performance of the crystalline **DHPP-3** having PF_6^- closely resembled those observed with the **DHPP-3** having I^-, demonstrating that the nature of the counter-anion exerts minimal impact on the switching properties (Fig. S25 and S26).

Switching upon far-red photon (740 nm) activation

It is noteworthy to mention that the modified phospho-**DHP**s (**DHPPs 1–3**) could be activated with red light (640 nm LED or 671 nm LASER). However, the activation of these derivatives by photons of wavelength > 700 nm (*i.e.* by far-red photons) could not be achieved. Our *in silico* studies with the help of DFT calculations (see later) and the previous reports[36,51] indicated that attaching even a moderate electron-donating group at the position directly conjugated with the electron-withdrawing phosphonium (4, 9-relation) could enable the switching of the

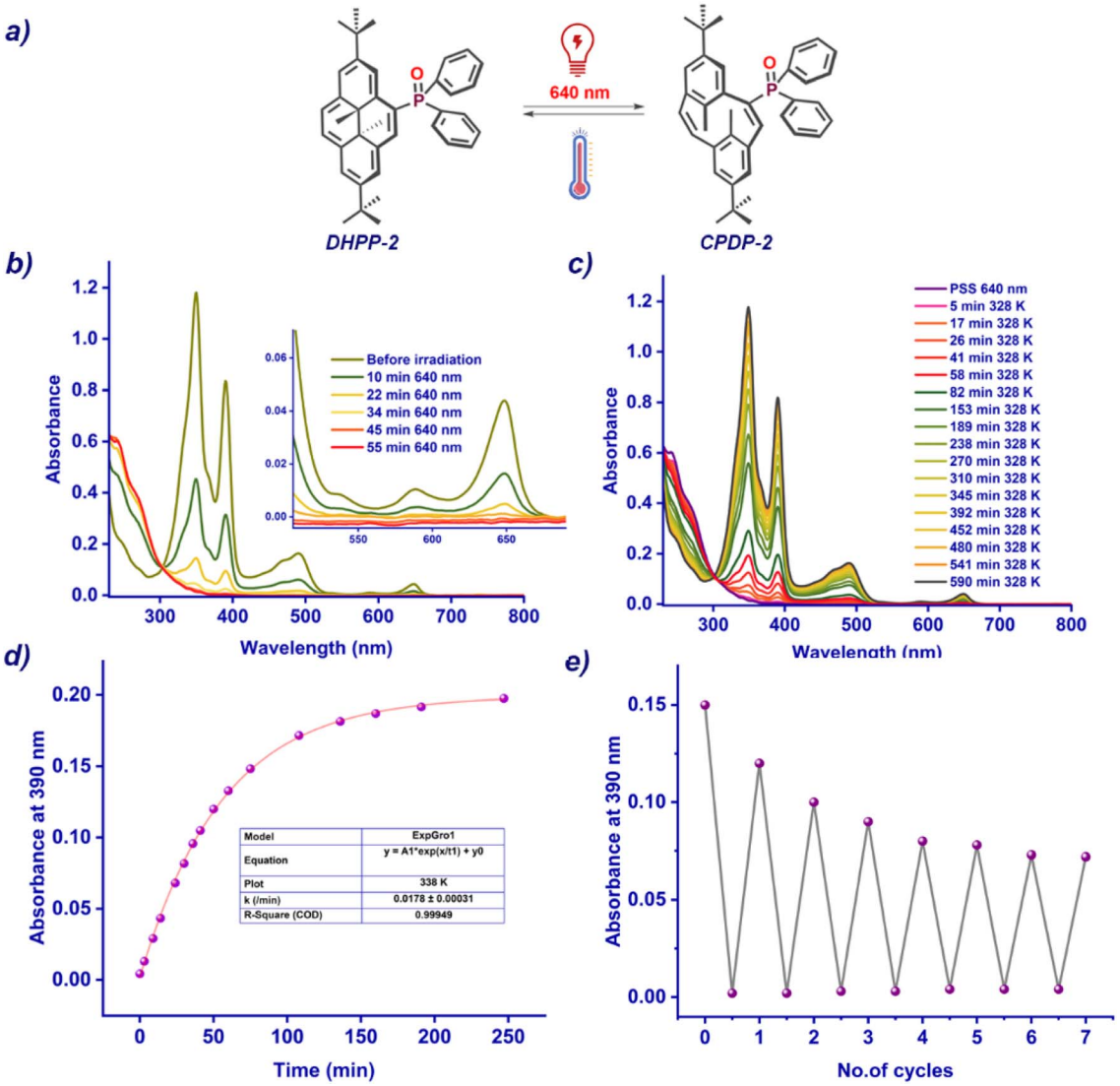

Fig. 3 (a) Schematic representation of photoisomerization and thermal reversal of DHPP-2. (b) Forward photoisomerization of DHPP-2 (30 micromolar in acetonitrile) upon 640 nm red light irradiation. (c) Thermal reverse isomerization for the formation of the DHPP-2 isomer at 328 K in acetonitrile. (d) Thermal reverse isomerization kinetics for the formation of the DHPP-2 isomer at 338 K in acetonitrile. (e) Photoswitching stability test of DHPP-2 upon forward isomerization with 640 nm light and reversal with 254 nm light.

system with >700 nm far-red light. Accordingly, we synthesized the compound **DHPP-4** (Scheme S1), attaching a moderate electron-donating acetamido (–NHCOCH$_3$) group opposite to the electron-withdrawing phosphonium salt to verify the hypothesis. This small variation greatly impacts the photophysical properties of the **DHPP-4**. The (moderate) donor–acceptor attachment directly conjugated at the 9-position of the **DHP** ring caused an expected downfield shift of the resonance frequency of the internal methyl groups compared to **DHPP-1** or **DHPP-3**. Thus, in ^{1}H NMR, the internal methyl protons appeared at −3.75 ppm for **DHPP-4** in comparison to **DHPP-1**, where the internal methyl protons appeared at around −3.95 and −3.97 ppm. Interestingly, all the absorption bands of **DHPP-4** were also red-shifted in comparison to those of **DHPP-1**, so it can be activated with far-red light in water (Fig. 4c and d). Indeed, the ring-opening of **DHPP-4** to **CPDP-4** can be achieved quantitatively upon excitation with 740 nm far-red photons at a moderate speed, even upon irradiating at the extreme tail-end of the S_1-band ($\varepsilon \sim 50$ M^{-1} cm^{-1} at 740 nm). The forward isomerization can also be performed with 640 nm red light, and the reversal can be accomplished by 427 nm blue light (Fig. S35) or with 254 nm UV, as well as thermally, similarly to the other cationic derivatives (Fig. 4b and d). The PSS distributions and the ring-opening quantum yield are tabulated in Table 1. The thermal reversal of the **CPDP-4** was almost quantitative, with an activation energy barrier of 21.25 ± 0.57 kcal mol^{-1}, corresponding to a thermal half-life of the metastable **CPDP-4** of ∼10 h at 298 K (Table 1). Thus, **DHPP-4** demonstrated a successful design strategy *via* the introduction of a donor–

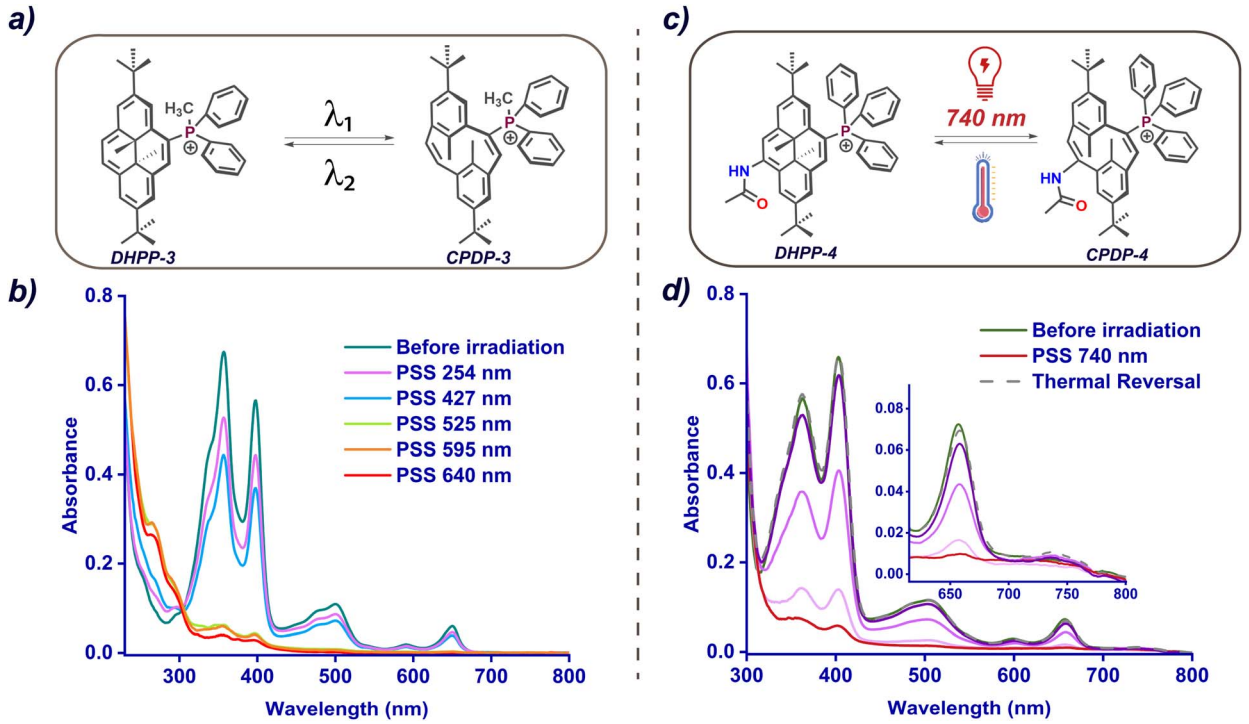

Fig. 4 (a) Schematic representation of photoisomerization of **DHPP-3** (I^- as the counteranion). (b) PSS distribution of photoswitching of **DHPP-3** upon irradiation with light of various wavelengths. (c) Schematic representation of photoisomerization of **DHPP-4** (Br^- as the counteranion). (d) Photoisomerisation of **DHPP-4** to **CPDP-4** (30 μM in 100 mM PBS buffer) at pH 7.2.

acceptor system that enabled efficient photoswitching of the system in water with far-red photons (740 nm).

Switching in buffer media

The ability of far-red light (740 nm) mediated switching of **DHPP-4** prompted us to investigate its switching behavior in a buffer of biological pH for prospective biological applications. In PBS buffer (phosphate-buffered saline) of pH 7.4 (100 mM), the compound was stable and exhibited quantitative forward switching upon 740 nm light, along with near-quantitative back switching upon thermal activation (Fig. 4d, S27 and S28). The reversal could also be performed by photo-activation, and ~80% of the reversal was observed upon 254 nm light irradiation. Additionally, we have also checked the photoswitching activity of **DHPP-4** in two other buffers of pH 5.6 (acetate buffer, 100 mM) and 8.6 (PBS buffer, 100 mM). To our delight, we observed quantitative forward switching upon 740 nm light irradiation followed by near-quantitative thermal reversal (Fig. S29–S32).

Theoretical investigation

To elucidate the role of directly attached cationic phosphorus in the improved photochemical performance of the novel **DHPP** systems, detailed theoretical calculations were conducted using density functional theory (DFT) methods. The ground-state structures of all the synthesized compounds, including the parent **DHP-H** as a model, were optimized using B3LYP/6-311G (d,p) with a PCM solvent model in water (see the SI for calculation details, Table S8). TD-DFT calculations were performed (employing **DHP-H** as a reference system, Fig. 1) to unravel the absorption profiles of the synthesized derivatives using a long-range corrected hybrid ωB97XD functional in conjunction with the 6-311G(d,p) basis set.[50] For **DHP-H**, the vertical excitations calculated for the two lowest energy bands appeared at 588 nm ($S_0 \rightarrow S_1$) and 502 nm ($S_0 \rightarrow S_2$), with oscillator strengths of 0.008 and 0.087, respectively (Table S9). Unlike **DHP-H**, for these newly modified derivatives, the vertical excitations of the two lowest energy bands ($S_0 \rightarrow S_1/S_0 \rightarrow S_2$) were estimated to be 596/511 nm for **DHPP-1**, 593/509 nm for **DHPP-3**, 607/514 nm for **DHPP-4** and 596/508 for **DHPP-2**, with substantially high oscillator strengths of 0.046/0.046, 0.045/0.044, 0.05/0.046 and 0.026/0.06, respectively (Table S9). All computed vertical transition energies fall within the expected TD-DFT accuracy (error < 0.3 eV) relative to the experiment.[63] The marked increase in the oscillator strengths for $S_0 \rightarrow S_1$ transitions in the modified cationic **DHPPs** indicates enhanced probability of photoswitching even upon activation with lower-energy red light, provided that the S_1 state acquires the essential zwitterionic character (*vide infra*) necessary for **DHP** → **CPD** photoisomerization. Generally, for normal **DHP**, the S_1 state corresponds to a locally excited (LE) state, while the S_2 state is identified as the active zwitterionic (Z) state characterized by an elongated transannular bond, and the latter is essentially responsible for the **DHP** → **CPD** photoisomerization.[49,64] Interestingly, the TD-DFT calculations on the modified **DHPPs** revealed an inversion of the LE and the Z characters in the excited-state ordering relative to the unmodified **DHP-H** system. The orbital composition of the S_1 state in the modified derivatives resembles that of the S_2 (*i.e.*, Z) state in **DHP-H**, while their

S_2 aligns with S_1 (*i.e.*, LE) of the **DHP-H** (Table S10). This inversion strongly suggests that the S_1 state in the modified **DHPPs** acquires the zwitterionic character necessary for efficient photoisomerization.

To further validate this inversion of the LE and the Z states in the newly synthesized **DHPP** derivatives, excited-state optimizations using the ωB97XD/6-311G (d,p) level of theory reveal a significant increase in the transannular C–C bond length (1.56–1.57 Å *vs.* 1.54 Å) (Fig. 1, see the bond marked with blue and Table S8) and a greater deviation from planarity in the charged compounds (Table S11), consistent with a zwitterionic S_1 state.[49,64] (Note: under the same theoretical model, no significant change in the transannular bond length was observed for normal **DHP-H**). Furthermore, for all the modified **DHPPs** the C–P bond shortened from 1.81–1.82 Å to 1.77 Å (Table S8), indicating their enhanced double-bond character and the presence of charge transfer in the S_1 excited state. Here, it is worth mentioning that the structural changes in the excited state are less pronounced for the neutral **DHPP-2** compared to the charged derivatives (Table S8). In particular, the longer C–P bond in the S_1 excited state of **DHPP-2** may be attributed to the unavailability of the appropriate acceptor orbitals in the already pentavalent phosphorus. This results in a less pronounced zwitterionic character in the S_1 state, which aligns well with the slower ring-opening observed for this neutral derivative.

To further rationalize the marked enhancement in the ring-opening quantum yield of the charged derivatives compared to that of the parent **DHP**, the evolution of the excited states (**DHP** → [**CPD***]) was studied, which revealed the key factors for the **DHP** → **CPD** photoisomerization efficiency.[49] As identified in the previous reports,[49,64,65] for the parent **DHP**, **CPD***, formation is suppressed by an efficient S_2 → S_1 internal conversion, leading to the lowest singlet excited state (LE state) and thus, **DHP** → **CPD** conversion requires irradiation at $\lambda >$ 430 nm accompanied by a low ring opening quantum yield.[62,65] However, interestingly, when the evolution of excited states was performed for one of our cationic derivatives, **DHPP-3**, it was found that the direct excitation to S_1 (Z-state) leads to **CPD*** formation without competing excited-state relaxation (Fig. S63). This finding is consistent with the experimental observations that **DHPP-3** → **CPDP-3** conversion upon irradiation at $\lambda >$ 640 nm was extremely efficient. The enhanced efficiency further supported that S_1 in **DHPP-3** acquired the zwitterionic character necessary for **CPD*** formation (see the SI for details of the calculation). Intriguingly, natural transition orbital (NTO) analysis of the first excited state, along with the corresponding oscillator strengths, also revealed an interesting correlation. For the slower **DHPP-2** ring opening, the transition responsible for imparting the zwitterionic character (**CPD*** formation) to S_1 contributes only 66% (Fig. 5), with half of the oscillator strength (*vide supra*) observed for the other three charged derivatives. In contrast, for the cationic **DHPP-1**, **DHPP-3**, and **DHPP-4**, this contribution increased to 78%, 83%, and 84%, respectively, closely matching the observed trend in the enhanced ring-opening efficiency. These analyses highlight how the presence of the charge modulates the excited-state dynamics of these

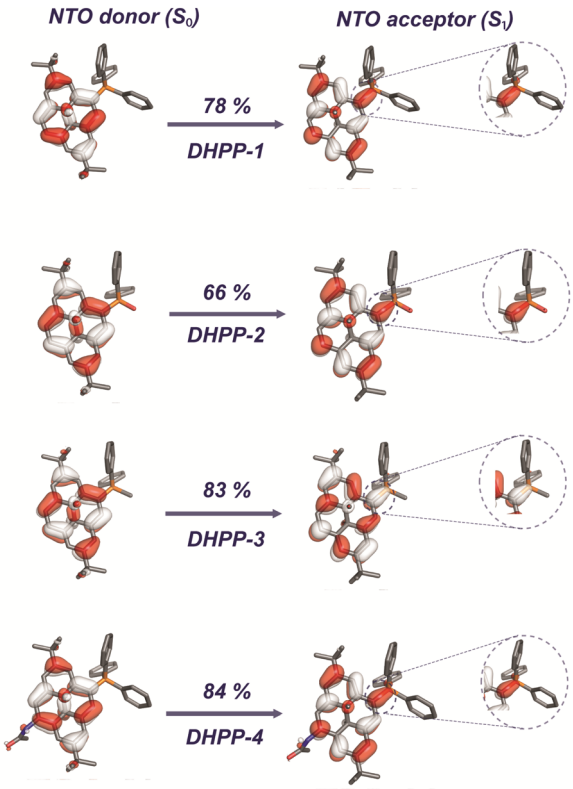

Fig. 5 Natural transition orbitals (NTOs) corresponding to the dominant component of the S_0 → S_1 transition, showing the donor (left) and acceptor (right) orbitals. Note the pronounced C=P double bond character in the acceptor orbital.

DHPPs, facilitating more efficient photoswitching in cationic phosphonium **DHPPs** compared to neutral **DHPP-2**.

Fluorescence properties

The attachment of the phosphonium moiety on the **DHP** scaffold was expected to cause significant alterations in the emission profile in the synthesized derivatives. Indeed, the emission spectra of all the phosphorus-modified **DHPPs** displayed significant bathochromic shifts compared to the parent **DHP**. Upon 370 nm excitation, the parent **DHP** (Scheme 1) exhibits an emission maximum at 647 nm, whereas **DHPP-1**, **DHPP-2**, **DHPP-3**, and **DHPP-4** display red-shifted emission maxima at 658 nm, 654 nm, 656 nm, and 665 nm, respectively (Fig. S60). Interestingly, all the synthesized derivatives have broad red-shifted emission spectra that tail out up to 800 nm, which aligns with the TD-DFT calculated emission (Table S7). The theoretical and experimental emission wavelengths, along with the relative fluorescence quantum yields, are provided in the SI (Table S7).

All-photonic orthogonal switching

Encouraged by the excellent switching of the phosphonium salts (**DHPP-1**, **3**, **4**) in water upon red (640 nm) and far-red (740 nm) light activation, we explored the orthogonal switching behaviour of a mixture of unsubstituted **DHP** and the cationic phosphonium **DHPPs** (Fig. 6a). While the normal unsubstituted **DHP**

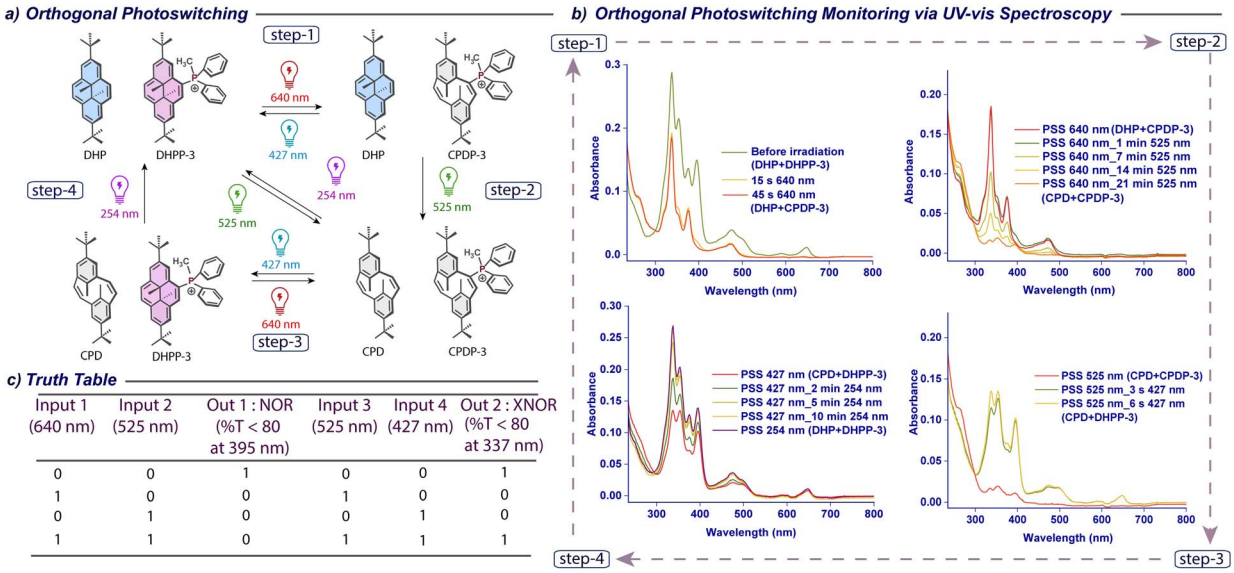

c) Truth Table

Input 1 (640 nm)	Input 2 (525 nm)	Out 1 : NOR (%T < 80 at 395 nm)	Input 3 (525 nm)	Input 4 (427 nm)	Out 2 : XNOR (%T < 80 at 337 nm)
0	0	1	0	0	1
1	0	0	1	0	0
0	1	0	0	1	0
1	1	0	1	1	1

Fig. 6 All-photonic orthogonal photoswitching of **DHP** and **DHPP-3** in molecular logic applications. (a) Schematic representation of all-photonic orthogonal photoisomerization of a mixture of **DHP** and **DHPP-3** (I^- as the counteranion). (b) UV-vis absorption spectral changes during orthogonal photoswitching and corresponding isomer enrichments in the PSS in methanol. (c) Truth table for different logic gates under various wavelengths of light as inputs and defined changes in the % transmittance (% *T*) as outputs.

undergoes forward switching with up to 525 nm light and reverts with 254 nm UV light, the **DHPPs** can be isomerized in the forward direction upon exposure to 640–740 nm light, and the reverse reaction can be accomplished with 427 nm blue light. Considering the comparable reverse switching PSS distribution of **DHPP-3** under both 427 nm and 254 nm light irradiation, we set out to explore the all-photonic orthogonal switching behaviour of a 1 : 1 mixture of **DHP** and **DHPP-3**. First, cationic **DHPP-3** was quantitatively opened to generate **CPDP-3** upon 640 nm red light activation keeping the ring-opening of **DHP** unaffected (Fig. 6b). After that, the ring-opening of **DHP** was accomplished in a quantitative manner producing open **CPD** upon 525 nm green light activation (Fig. 6b). The reversal of **CPDP-3** can be attained almost instantly with 427 nm blue light leading to the "closed" **DHPP-3** (Fig. 6b) and leaving the "open" **CPD** intact. Finally, the **CPD** isomer was converted to the respective closed **DHP** in a quantitative manner upon 254 nm UV light irradiation (Fig. 6b). Thus, four clean, efficient photoconversions without cross-reactivity were obtained by sequential irradiation at 640 nm, 525 nm, 427 nm, and 254 nm. This demonstrates the use of light inputs alone to achieve precise, wavelength-encoded molecular control. Finally, with the orthogonal photoswitching system in our hand, we set out to customize all-photonic molecular logic operations. By employing two different sets of selected wavelength inputs and monitoring changes in the percentage transmittance (% *T*) at a suitable wavelength in the UV-vis spectra as outputs, construction of different logic gates like NOR and XNOR was demonstrated (Fig. 6c).

Conclusions

In summary, we have synthesized a series of previously unexplored dimethyldihydropyrene phosphonium salts (**DHPPs**) displaying improved photoswitching upon red and even far-red light activation in a quantitative fashion. The fully aqueous operative nature, along with fast, efficient photoisomerisation, makes this modified photochromic system a promising candidate for water-soluble photoswitches capable of operating in the biological window. In-depth theoretical calculations offer coherent explanations for the improved photophysical properties of these modified systems, consistent with the experimental observations. In addition to that, an all-photonic orthogonal switching behaviour was accomplished with a mixture of conventional **DHP** and one of our phosphonium **DHPP** derivatives, demonstrating the construction of various all-photonic molecular logic operations. Further development of the next generation of phosphonium-based dimethyl dihydropyrenes is underway in our laboratory.

Experimental

Detailed synthetic procedures and analyses of presented compounds, NMR spectra, crystallographic data, and photophysical studies, including Fig. S1–S63, Scheme S1 and Tables S1–S11 (PDF).

Author contributions

S. B. initiated the work by conceptualization, funding acquisition, investigation, methodology, resources, writing, and editing. M. L. M. performed synthesis, photophysical studies, writing and editing. M. L. M. and S. C. performed the photophysical studies and analysis. S. M. performed the theoretical investigation, writing and editing. The manuscript was written through the contributions of all authors. All authors have approved the final version of the manuscript.

Conflicts of interest

There are no conflicts to declare.

Data availability

CCDC 2444320 and 2442745 contain the supplementary crystallographic data for this paper.[66]

The data that support the findings of this study are available in the supplementary information (SI) of this article. Supplementary information is available. See DOI: https://doi.org/10.1039/d5sc06168g.

Acknowledgements

This work is funded by SERB (ANRF) (Grant No. SERB/CRG/2022/006776 to S. B.). M. L. M. and S. C. are both supported by a fellowship from CSIR, India. S. M. is supported by a fellowship from NSERC and MITACS, Canada. S. M. thanks Dr Tim Storr and the Digital Research Alliance of Canada for supercomputer access. The authors acknowledge Dr Saikat Mondal and Dr Prathapa Siriyara Jagannatha for their assistance with the SC-XRD analysis.

Notes and references

1 A. Mourot, I. Tochitsky and R. H. Kramer, *Front. Mol. Neurosci.*, 2013, **6**, 5.
2 T. Fehrentz, M. Schönberger and D. Trauner, *Angew. Chem., Int. Ed.*, 2011, **50**, 12156–12182.
3 P. Paoletti, G. C. R. Ellis-Davies and A. Mourot, *Nat. Rev. Neurosci.*, 2019, **20**, 514–532.
4 M. W. H. Hoorens and W. Szymanski, *Trends Biochem. Sci.*, 2018, **43**, 567–575.
5 L. Li, A. A. Shemetov, M. Baloban, P. Hu, L. Zhu, D. M. Shcherbakova, R. Zhang, J. Shi, J. Yao, L. V. Wang and V. V. Verkhusha, *Nat. Commun.*, 2018, **9**, 2734.
6 R. McQuillen, A. J. Perez, X. Yang, C. H. Bohrer, E. L. Smith, S. Chareyre, H. C. T. Tsui, K. E. Bruce, Y. M. Hla, J. W. McCausland, M. E. Winkler, E. D. Goley, K. S. Ramamurthi and J. Xiao, *Nat. Commun.*, 2024, **15**, 10746.
7 F. Bierbuesse, A. C. Bourges, V. Gielen, V. Mönkemöller, W. Vandenberg, Y. Shen, J. Hofkens, P. V. Berghe, R. E. Campbell, B. Moeyaert and P. Dedecker, *Nat. Commun.*, 2022, **13**, 1850.
8 D. Evanko, *Nat. Methods*, 2008, **5**, 23.
9 K. Zhang and B. Cui, *Trends Biotechnol.*, 2015, **33**, 92–100.
10 R. Dorel and B. L. Feringa, *Chem. Commun.*, 2019, **55**, 6477–6486.
11 S. Adak, M. L. Maity and S. Bandyopadhyay, *ACS Omega*, 2022, **7**, 35361–35370.
12 M. Saha, M. S. Hossain and S. Bandyopadhyay, *Angew. Chem., Int. Ed.*, 2021, **60**, 5220–5224.
13 M. Saha, P. Jana and S. Bandyopadhyay, *Angew. Chem., Int. Ed.*, 2025, **64**, e202509194.
14 P. Kobauri, F. J. Dekker, W. Szymanski and B. L. Feringa, *Angew. Chem., Int. Ed.*, 2023, **62**, e202300681.
15 K. Hüll, J. Morstein and D. Trauner, *Chem. Rev.*, 2018, **118**, 10710–10747.
16 W. A. Velema, W. Szymanski and B. L. Feringa, *J. Am. Chem. Soc.*, 2014, **136**, 2178–2191.
17 A. A. Beharry and G. A. Woolley, *Chem. Soc. Rev.*, 2011, **40**, 4422–4437.
18 S. Crespi, N. A. Simeth and B. König, *Nat. Rev. Chem.*, 2019, **3**, 133–146.
19 R. Klajn, *Chem. Soc. Rev.*, 2014, **43**, 148–184.
20 M. Mostaghimi, H. P. Hernandez, Y. Jiang, W. Wenzel, L. Heinke and M. Kozlowska, *Commun. Chem.*, 2023, **6**, 275.
21 S. Kar, S. Chatterjee and S. Bandyopadhyay, *Synthesis*, 2024, **57**, 189–195.
22 J. Wang, X. Liu, J. Wang, F. Li, H. Jiang and L. Liu, *Luminescence*, 2024, **39**, e4546.
23 J. C. H. Chan, W. H. Lam and V. W. W. Yam, *J. Am. Chem. Soc.*, 2014, **136**, 16994–16997.
24 J. Volarić, W. Szymanski, N. A. Simeth and B. L. Feringa, *Chem. Soc. Rev.*, 2021, **50**, 12377–12449.
25 M. L. Maity, S. Mahato and S. Bandyopadhyay, *Angew. Chem., Int. Ed.*, 2023, **62**, e202311551.
26 M. Fink, J. Stäuble, M. Weisgerber and E. M. Carreira, *J. Am. Chem. Soc.*, 2024, **146**, 9519–9525.
27 A. K. Gaur, D. Gupta, D. N. Nampoothiry, A. Velloth, R. Kaur, N. Kaur and S. Venkataramani, *Chem. Eur J.*, 2024, **30**, e202401239.
28 D. V. Berdnikova, *Chem. Eur J.*, 2024, **30**, e202304237.
29 D. Puthoff, H. Kuttiyil and J. A. Peterson, *J. Am. Chem. Soc.*, 2024, **146**, 34008–34013.
30 F. Kohl, T. Vogl, F. Hampel and H. Dube, *Nat. Commun.*, 2025, **16**, 1760.
31 S. Koppayithodi, P. Jana and S. Bandyopadhyay, *J. Org. Chem.*, 2025, **90**, 4518–4524.
32 A. K. Gaur, D. Gupta, A. Mahadevan, P. Kumar, H. Kumar, D. N. Nampoothiry, N. Kaur, S. K. Thakur, S. Singh, T. Slanina and S. Venkataramani, *J. Am. Chem. Soc.*, 2023, **145**, 10584–10594.
33 Y. Yang, R. P. Hughes and I. Aprahamian, *J. Am. Chem. Soc.*, 2014, **136**, 13190–13193.
34 S. Helmy, F. A. Leibfarth, S. Oh, J. E. Poelma, C. J. Hawker and J. R. de Alaniz, *J. Am. Chem. Soc.*, 2014, **136**, 8169–8172.
35 S. Bandyopadhyay, in *Molecular Photoswitches: Chemistry, Properties, and Applications,* 2022, vol. 1–2, pp. 193–212.
36 K. Klaue, Y. Garmshausen and S. Hecht, *Angew. Chem., Int. Ed.*, 2018, **57**, 1414–1417.
37 H. Kuroiwa, Y. Inagaki, K. Mutoh and J. Abe, *Adv. Mater.*, 2019, **31**, 1805661.
38 K. Mutoh, M. Sliwa and J. Abe, *J. Phys. Chem. C*, 2013, **117**, 4808–4814.
39 Y. Zheng, Y. Meana, M. M. A. Mazza, J. D. Baker, P. J. Minnett and F. M. Raymo, *J. Am. Chem. Soc.*, 2022, **144**, 4759–4763.
40 N. Ishii, T. Kato and J. Abe, *Sci. Rep.*, 2012, **2**, 819.
41 Y. Kobayashi and J. Abe, *Adv. Opt. Mater.*, 2016, **4**, 1354–1357.
42 H. R. Blattmann, D. Meuche, E. Heilbronner, R. J. Molyneux and V. Boekelheide, *J. Am. Chem. Soc.*, 1965, **87**, 130–131.

43 M. Tashiro and T. Yamato, *J. Am. Chem. Soc.*, 1982, **104**, 3701–3707.
44 R. H. Mitchell, T. R. Ward, Y. Chen, Y. Wang, S. A. Weerawarna, P. W. Dibble, M. J. Marsella, A. Almutairi and Z. Q. Wang, *J. Am. Chem. Soc.*, 2003, **125**, 2974–2988.
45 K. Ayub, R. Li, C. Bohne, R. V. Williams and R. H. Mitchell, *J. Am. Chem. Soc.*, 2011, **133**, 4040–4045.
46 Z. Ziani, F. Loiseau, E. Lognon, M. Boggio-Pasqua, C. Philouze, S. Cobo and G. Royal, *Chem. Eur J.*, 2021, **27**, 16642–16653.
47 A. Bakkar, S. Cobo, F. Lafolet, D. Roldan, E. Saint-Aman and G. Royal, *J. Mater. Chem. C*, 2016, **4**, 1139–1143.
48 M. Jacquet, F. Lafolet, S. Cobo, F. Loiseau, A. Bakkar, M. Boggio-Pasqua, E. Saint-Aman and G. Royal, *Inorg. Chem.*, 2017, **56**, 4357–4368.
49 D. Roldan, S. Cobo, F. Lafolet, N. Vilà, C. Bochot, C. Bucher, E. Saint-Aman, M. Boggio-Pasqua, M. Garavelli and G. Royal, *Chem. Eur J.*, 2015, **21**, 455–467.
50 Z. Ziani, S. Cobo, F. Loiseau, D. Jouvenot, E. Lognon, M. Boggio-Pasqua and G. Royal, *JACS Au*, 2023, **3**, 131–142.
51 K. Klaue, W. Han, P. Liesfeld, F. Berger, Y. Garmshausen and S. Hecht, *J. Am. Chem. Soc.*, 2020, **142**, 11857–11864.
52 X. L. Chen, X. D. Tao, Y. S. Wang, Z. Wei, L. Meng, D. H. Zhang, F. L. Lin and C. Z. Lu, *CCS Chem.*, 2023, **5**, 589–597.
53 A. Belyaev, Y. Cheng, Z. Liu, A. J. Karttunen, P. Chou and I. O. Koshevoy, *Angew. Chem., Int. Ed.*, 2019, **58**, 13456–13465.
54 A. Belyaev, B. K. Su, Y. H. Cheng, Z. Y. Liu, N. M. Khan, A. J. Karttunen, P. T. Chou and I. O. Koshevoy, *Angew. Chem., Int. Ed.*, 2022, **61**, e202115690.
55 T. Werner, *Adv. Synth. Catal.*, 2009, **351**, 1469–1481.
56 J. Zielonka, J. Joseph, A. Sikora, M. Hardy, O. Ouari, J. Vasquez-Vivar, G. Cheng, M. Lopez and B. Kalyanaraman, *Chem. Rev.*, 2017, **117**, 10043–10120.
57 C. Hansch, A. Leo and R. W. Taft, *Chem. Rev.*, 1991, **91**, 165–195.
58 I. Partanen, A. Belyaev, B. K. Su, Z. Y. Liu, J. J. Saarinen, I. I. Hashim, A. Steffen, P. T. Chou, C. Romero-Nieto and I. O. Koshevoy, *Chem. Eur J.*, 2023, **29**, e202301073.
59 R. H. Mitchell and T. R. Ward, *Tetrahedron*, 2001, **57**, 3689–3695.
60 D. Marcoux and A. B. Charette, *J. Org. Chem.*, 2008, **73**, 590–593.
61 C. E. Weston, R. D. Richardson, P. R. Haycock, A. J. P. White and M. J. Fuchter, *J. Am. Chem. Soc.*, 2014, **136**, 11878–11881.
62 M. A. L. Sheepwash, R. H. Mitchell and C. Bohne, *J. Am. Chem. Soc.*, 2002, **124**, 4693–4700.
63 A. D. Laurent and D. Jacquemin, *Int. J. Quantum Chem.*, 2013, **113**, 2019–2039.
64 M. Boggio-Pasqua and M. Garavelli, *J. Phys. Chem. A*, 2015, **119**, 6024–6032.
65 M. Boggio-Pasqua, M. J. Bearpark and M. A. Robb, *J. Org. Chem.*, 2007, **72**, 4497–4503.
66 (*a*) CCDC 2444320: Experimental Crystal Structure Determination, 2025, DOI: **10.5517/ccdc.csd.cc2n1j19**; (*b*) CCDC 2442745: Experimental Crystal Structure Determination, 2025, DOI: **10.5517/ccdc.csd.cc2mzw7r**.